Research Square

Preprints are preliminary reports that have not undergone peer review.
They should not be considered conclusive, used to inform clinical practice,
or referenced by the media as validated information.

ISAR Imaging Method of High-Speed Maneuvering Multi-Targets Based on Improved Keystone Transform and FrFT

CHEN Siyuan
Shijiazhuang Campus of Army Engineering University
HU Wenhua
cccg006306153.com
Shijiazhuang Campus of Army Engineering University
GUO Baofeng
Shijiazhuang Campus of Army Engineering University
XUE Dongfang
Shijiazhuang Campus of Army Engineering University
LI Miao
Shijiazhuang Campus of Army Engineering University

Research Article

Keywords: ISAR, high-speed maneuvering target, multi-target imaging, Keystone transform, FrFT, motion compensation, global coordinate reconstruction

Posted Date: November 26th, 2026

DOI: https://doi.org/10.21203/rs.3.rs-11669887/v1

License: This work is licensed under a Creative Commons Attribution 4.0 International License.
Read Full License

Additional Declarations: No competing interests reported.

ISAR Imaging Method of High-Speed Maneuvering Multi-Targets Based on Improved Keystone Transform and FrFT

CHEN Siyuan, HU Wenhua[1]*, GUO Baofeng, XUE Dongfang, LI Miao

(Shijiazhuang Campus of Army Engineering University,Shijiazhuang Hebei 050003,China)

Abstract: To address the problems of severe range migration, difficulty in motion parameter estimation, and echo coupling among multiple targets in high-speed maneuvering multi-target inverse synthetic aperture radar (ISAR) imaging, a multi-high-speed maneuvering target ISAR imaging and global coordinate reconstruction method based on improved Keystone transform and fractional Fourier transform (FrFT) is proposed. The proposed method first obtains target motion trajectories through peak detection after range compression and establishes parameter estimation constraints using a second-order motion model. A generalized second-order Keystone transform is employed to correct the quadratic range curvature induced by target acceleration, while the energy focusing property of the FrFT domain is exploited to estimate the radial acceleration of targets and achieve multi-target parameter association using trajectory information. Subsequently, acceleration compensation and first-order Keystone transform are utilized to recover target velocities and construct complete motion models. A target-by-target translational motion compensation strategy combined with joint gating is further adopted to separate echoes from multiple targets. Finally, the mapping relationship between the local coordinate system and the global coordinate system is established according to the estimated target motion parameters, enabling multi-target ISAR image fusion and spatial position reconstruction. Simulation results demonstrate that the proposed method can effectively estimate the motion parameters of high-speed maneuvering targets, suppress range migration caused by velocity and acceleration, and achieve independent ISAR imaging and global coordinate reconstruction of multiple targets, verifying its effectiveness in complex multi-target high-speed maneuvering scenarios.

Keywords: ISAR; high-speed maneuvering target; multi-target imaging; Keystone transform; FrFT; motion compensation; global coordinate reconstruction

I. Introduction

ISAR utilizes the relative motion between the target and radar to form an equivalent aperture, thereby achieving high-resolution imaging in range and cross-range dimensions through echo signal processing[1][2]. It has been widely applied in non-cooperative target recognition, space target surveillance, and complex battlefield environment monitoring. However, with the continuous improvement in maneuverability and stealth capabilities of modern targets,

[1] Correspponging author: Wenhua Hu is with the Shijiazhuang Campus, Army Engineering University, Shijiazhuang 050003, China (e-mail: cccg00630@163.com).

ISAR imaging under complex maneuvering conditions faces increasingly severe challenges[3].

Traditional Range-Doppler(RD) algorithms assume that the target undergoes uniform motion within a coherent processing interval(CPI)[4][5]. When the target moves at a constant velocity, the scattered echoes exhibit stable range migration characteristics. However, when the target performs accelerated motion, range migration becomes more complicated, resulting in residual phase errors after motion compensation[6][7]. Moreover, for highly maneuvering targets, multiple scattering centers may simultaneously exist within the radar beam coverage, and different scattering centers may possess different motion parameters. This causes range-dependent Doppler coupling effects, increasing the difficulty of motion parameter estimation and target imaging[8][9].

To address range migration issues, Keystone transformation has been widely applied for motion compensation. Traditional Keystone methods mainly focus on uniformly moving targets, while the range migration caused by high-speed maneuvering targets remains difficult to completely correct[10][11]. Recently, improved Keystone-based approaches have been proposed to compensate for complex motion-induced range migration. However, due to differences in velocity and acceleration parameters among scattering centers, a single motion compensation model is difficult to adapt to all targets[12][13].

Furthermore, the echo signals of high-speed maneuvering targets usually contain linear frequency modulation(LFM) components caused by quadratic phase terms. FrFT can achieve energy aggregation of LFM signals in the fractional Fourier domain and has therefore been widely applied in maneuvering target parameter estimation[14][15]. However, under multi-target conditions, multiple targets may overlap in the FrFT domain, making it difficult to accurately distinguish target identities using only motion parameter estimation based on FrFT[16][17].

To overcome the above limitations, this paper proposes a multi-target ISAR imaging method based on the joint processing of improved Keystone transformation and FrFT, enabling complete parameter estimation and imaging of high-speed maneuvering targets. First, the proposed method employs a range alignment strategy to estimate multiple target trajectories and establishes a two-dimensional motion model to characterize the complex motion characteristics of maneuvering targets. Subsequently, a nonlinear Keystone transformation is introduced to correct range migration caused by acceleration and higher-order motion components. Meanwhile, FrFT is utilized to estimate the cross-range acceleration parameters, and multi-target parameter association is achieved through trajectory tracking. Based on this framework, a complete motion compensation model is constructed, followed by ISAR imaging using the adaptive Keystone transformation and coherent integration strategy. Finally, the target position reconstruction is achieved through image registration and spatial coordinate mapping, enabling accurate multi-target ISAR imaging under complex maneuvering conditions.

II. Multi-target Echo Signal Model for ISAR

A. Radar Transmitted Signal and Echo Modeling

ISAR exploits the relative motion between the target and radar to generate an equivalent aperture, and achieves two-dimensional high-

resolution imaging of non-cooperative targets through range–Doppler processing of target echoes. However, in practical complex detection scenarios, multiple maneuvering targets often simultaneously exist within the radar observation region. Since different targets exhibit distinct motion states, the received echo signals suffer from severe challenges, including range migration, range curvature, and multi-target coupling effects.

For high-speed moving targets, when velocity exists, the target scattering centers undergo linear displacement along the range direction, causing the echo energy to span across multiple range cells. When acceleration is involved, the range variation further exhibits a quadratic dependence on slow time, resulting in curved range migration trajectories. Conventional ISAR imaging methods based on the RD algorithm generally assume that the target motion is approximately uniform. Therefore, severe image defocusing may occur in the presence of acceleration or multiple targets. The geometric relationship of multi-target ISAR imaging is illustrated in Fig. 1.

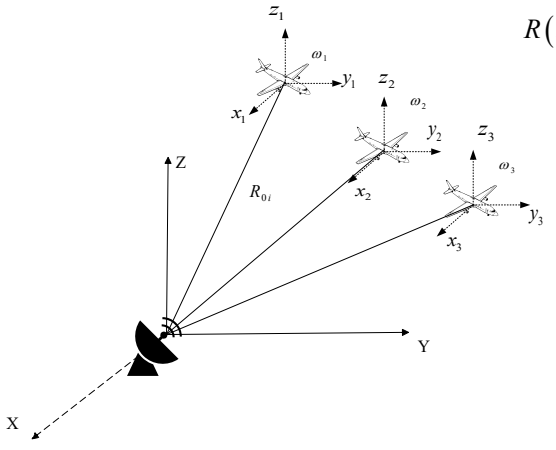


Fig. 1. Imaging geometry of multi-target ISAR.

The ISAR radar generally transmits a LFM signal to improve range resolution. The expression of the transmitted signal can be written as:

$$s(\hat{t},t_m)=rect(\frac{\hat{t}}{T_p}) \exp\left[j2\pi(f_c t+\frac{1}{2}\mu\hat{t}^2)\right] \tag{1}$$

where $rect(\cdot)$ denotes the rectangular window function, T_p represents the pulse width, f_c is the carrier frequency, and $\mu=\frac{B}{T_p}$ is the chirp rate, B denotes the signal bandwidth, $t_m=m\cdot PRT\left(m=0,1,2,...\right)$ represents the slow time, and PRT is the pulse repetition time. $\hat{t}$ denotes the fast time, while t represents the total time. The relationship between them satisfies $\hat{t}=t-t_m$.

After receiving the target-reflected echoes, the radar performs quadrature demodulation and sampling to obtain the baseband signal. For a point target located at an instantaneous range $R(t)$ its baseband echo can be expressed as:

$$s_r\left(t,t_m\right)=\sigma rect\left(\frac{t-\frac{2R(t)}{c}}{T_p}\right) \exp\left(-j\frac{4\pi R(t)}{\lambda}\right)\exp\left[j\pi\mu\left(\hat{t}-\frac{2R(t)}{c}\right)^2\right] \tag{2}$$

where σ denotes the complex reflection coefficient of the scattering center, c represents the speed of light, $\lambda=\frac{c}{f_c}$ is the wavelength. In (2), the first exponential term

represents the motion-induced phase modulation caused by target movement, while the second exponential term corresponds to the range-dependent frequency modulation term.

B. Multi-target Multi-scattering Center Echo Synthesis Model

In practical scenarios, multiple targets (such as fighter formations or missile groups) may simultaneously exist within the radar beam coverage. Each target can be modeled as being composed of I_k dominant scattering centers, as illustrated in Fig. 2, which shows the multi-target scattering center model for ISAR imaging.

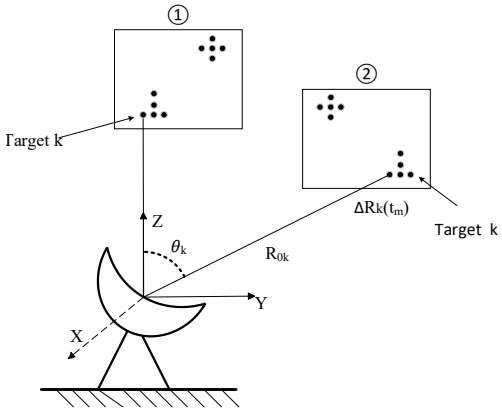


Fig. 2. Multi-target scattering center model for ISAR imaging.

Assume that the k-th target has an initial geometric center range of $R_{0,k}$, velocity v_k, acceleration a_k, and an initial rotation center position of $(x_{0,k}, y_{0,k})$. The azimuth position of the rotation center at slow time t_m can be expressed as:

$$x_{0,k}(t_m) = x_{0,k} + v_k t_m + \frac{1}{2} a_k t_m^2 \quad (3)$$

In the ISAR observation geometry, the angular variation of the target relative to the radar line of sight (LOS) is generally small. Therefore, the instantaneous slant range of the i-th scattering center on the k-th target can be expressed as:

$$R_{k,i}(t_m) = R_{0,k} + v_k t_m + \frac{1}{2} a_k t_m^2 + x_{k,i} \sin(\omega t_m) + y_{k,i} \cos(\omega t_m) \quad (4)$$

where ω denotes the equivalent rotation angular velocity of the target, which is determined by the equivalent rotational vector of the target relative to the radar. In ISAR imaging, the small-angle condition $\omega t_m \ll 1$ is usually satisfied. Therefore, the following small-angle approximation can be applied:

$$\sin(\omega t_m) \approx \omega t_m, \cos(\omega t_m) \approx 1 \quad (5)$$

Accordingly, the range equation after small-angle approximation becomes:

$$R_{k,i}(t_m) \approx R_{0,k} + y_{k,i} + v_k t_m + \frac{1}{2} a_k t_m^2 + x_{k,i} \omega t_m \quad (6)$$

It can be observed from the expanded range expression that the slant range contains both a linear term proportional to t_m and a quadratic term proportional to t_m^2. When the acceleration a_k cannot be ignored, the range trajectory of the scattering center exhibits significant curvature characteristics. Therefore, conventional envelope alignment methods based on linear motion models cannot effectively compensate for such nonlinear range migration.

By substituting (6) into the baseband echo model (2) and performing Fourier transform with respect to fast time to achieve pulse compression, while neglecting the amplitude variation caused by envelope attenuation after pulse compression, the compressed echo of the i-th scattering center on the k-th target can be represented in the range–slow time domain as:

$$\mathrm{s}_{k,i}\left(\hat{t},t_m\right)=\sigma_{k,i}\cdot rect\left(\frac{\hat{t}-2R_{k,i}\left(t_m\right)/c}{T_p}\right)\exp\left[j\pi\mu\left(\hat{t}-\frac{2R_{k,i}\left(t_m\right)}{c}\right)^2\right]\exp\left(-j\frac{4\pi f_c}{c}R_{k,i}\left(t_m\right)\right) \tag{7}$$

To achieve high range resolution, pulse compression processing is required along the fast-time dimension. Pulse compression is implemented in the frequency domain through matched filtering. Therefore, the Fourier transform is first performed with respect to the fast time $\hat{t}$, yielding the range-frequency domain signal as:

$$\mathrm{s}_{k,i}\left(f_\tau,t_m\right)=\sigma_{k,i}\cdot rect\left(\frac{f_\tau}{B}\right)\exp\left[-j\frac{4\pi}{c}\left(f_c+f_\tau\right)R_{k,i}\left(t_m\right)\right] \tag{8}$$

where f_τ is defined as $S\left(f_\tau\right)=\int_{-\infty}^{\infty}s\left(\hat{t}\right)e^{-j2\pi f_\tau\hat{t}}d\hat{t}$, which represents the range frequency variable corresponding to the fast-time frequency. By coherently summing the echoes from all targets and all scattering centers, the complete multi-target pulse-compressed echo signal model can be obtained as:

$$s\left(f_\tau,t_m\right)=\sum_{k=1}^{K}\sum_{i=1}^{I_k}\sigma_{k,i}\cdot rect\left(\frac{f_\tau}{B}\right)\exp\left[-j\frac{4\pi}{c}\left(f_c+f_\tau\right)R_{k,i}\left(t_m\right)\right] \tag{9}$$

Substituting (6) into the time-domain multi-target echo expression in (7), the influence of acceleration on the echo phase can be analyzed. By ignoring the higher-order terms introduced by the target rotation component, the echo phase can be approximately expressed as:

$$\phi_{k,i}\left(t_m\right)\approx-\frac{4\pi}{c}\left(f_c+f_\tau\right)\left(R_{0,k}+y_{k,i}+v_kt_m+\frac{1}{2}a_kt_m^2+x_{k,i}\omega t_m\right) \tag{10}$$

where the term v_kt_m corresponds to the linear range migration, the term $\frac{1}{2}a_kt_m^2$ represents the second-order range curvature caused by acceleration, and the term $x_{k,i}\omega t_m$ corresponds to the cross-range Doppler frequency induced by target rotation.

Due to the existence of acceleration, the motion parameter vector of each target is extended from the original form $\left(R_{0,k},\omega_k,v_k\right)$ to $\left(R_{0,k},\omega_k,v_k,a_k\right)$. Although the expansion of the parameter space increases the difficulty of parameter estimation, it also provides additional feature dimensions for signal separation. Specifically, the acceleration differences among different targets can be distinguished according to the peak locations in the FrFT domain, which provides the theoretical foundation for subsequent multi-target parameter estimation.

C. Range Migration Analysis

In a multi-target scenario with acceleration, the range migration of scattering centers is jointly determined by three physical mechanisms: linear range migration, second-order range curvature, and rotational components.

The phase term caused by the velocity v_k can be expressed as:

$$\phi_{v_k}\left(t_m\right)\approx-\frac{4\pi}{c}\left(f_c+f_\tau\right)v_kt_m=-\frac{4\pi}{c}f_cv_kt_m-\frac{4\pi}{c}f_\tau v_kt_m \tag{11}$$

where the first term $-\frac{4\pi}{c}f_cv_kt_m$ represents

the Doppler phase induced by the target uniform motion, which is an important signal component for cross-range focusing. The second term $-\frac{4\pi}{c} f_\tau v_k t_m$ describes the linear coupling between the range frequency and slow time. It indicates that different range-frequency components correspond to different Doppler frequencies. In the two-dimensional range–slow time plane, this phenomenon appears as a linear slant trajectory of the target. Considering the range resolution $\rho_a = \frac{c}{2B}$ and the coherent processing interval $T_a = M \cdot \mathrm{PRT}$ when $v_k \cdot T_a > \rho_a$, the target scattering center will migrate across multiple range cells, resulting in the MTRC phenomenon, which requires correction.

The phase term induced by the acceleration a_k can be expressed as:

$$\begin{aligned}\phi_{a_k}(t_m) &\approx -\frac{4\pi}{c}(f_c + f_\tau)\cdot\frac{1}{2}a_k t_m^2 \\ &= -\frac{2\pi}{c} f_c a_k t_m^2 - \frac{2\pi}{c} f_\tau a_k t_m^2\end{aligned} \tag{12}$$

where the first term $-\frac{2\pi}{c} f_c a_k t_m^2$ represents the Doppler modulation rate introduced by acceleration. It causes the cross-range phase to exhibit a quadratic variation and directly leads to cross-range defocusing in conventional RD imaging algorithms. The second term $-\frac{2\pi}{c} f_\tau a_k t_m^2$ describes the quadratic coupling between acceleration and range frequency. This term causes the range trajectory to exhibit parabolic curvature in the range–slow time domain, namely second-order range curvature. When $\frac{1}{2}a_k T_a^2 \square \rho_a$, the cross-range focusing performance will deteriorate significantly if the acceleration-induced phase error is not compensated.

The rotational motion of the target around its rotation center introduces a linear phase term proportional to the cross-range coordinate $x_{k,i}$ of the scattering center, which serves as the signal source for cross-range resolution. The first two motion components correspond to translational motion errors and should be removed before cross-range focusing. The third component represents the effective signal required for image formation. The core task of multi-target parameter estimation is to accurately estimate the velocity v_k and acceleration a_k of each target from the mixed echoes, thereby constructing the translational motion compensation function.

III. Multi-target ISAR Imaging Algorithm Based on Improved Keystone Transformation and FrFT

A. Multi-target Motion Parameter Estimation

1) Coarse Range Trajectory Estimation

To reduce the computational complexity of subsequent motion parameter searching, range peak detection is first performed on the two-dimensional range-compressed echo data. The initial range sequences of different targets along the slow time axis are obtained. Since the target motion within a CPI can be approximately modeled as uniformly accelerated motion, its range history can be expressed as:

$$R_k(t) = R_{0,k} + v_k t_m + \frac{1}{2}a_k t_m^2 \tag{13}$$

For the obtained range peak sequence, a second-order polynomial fitting method is employed to estimate the coarse range trajectory of each target:

$$\tilde{R}_k(t) = \tilde{R}_{0,k} + \tilde{v}_k t_m + \frac{1}{2}\tilde{a}_k t_m^2 \tag{14}$$

The motion parameters obtained from (14) are only used as coarse estimates rather than being directly applied for motion compensation. Instead, they are utilized for target trajectory association and provide initial parameter values and search ranges for the subsequent generalized second-order Keystone transformation and accurate FrFT-based parameter estimation.

By substituting (6) into the phase term of (9), and neglecting the rotational component and constant phase terms, the phase term introduced by translational motion can be expressed as:

$$\phi_{f_\tau}(f_\tau, t_m) = -\frac{4\pi}{c}(f_\tau + f_c)\left(v_k t_m + \frac{1}{2}a_k t_m^2\right) \tag{15}$$

Expanding (15), four terms can be obtained as:

$$\begin{aligned}\phi_{f_\tau}(f_\tau, t_m) = &-\frac{4\pi}{c}f_c v_k t_m - \frac{4\pi}{c}f_\tau v_k t_m \\ &-\frac{2\pi}{c}f_c a_k t_m^2 - \frac{2\pi}{c}f_\tau a_k t_m^2\end{aligned} \tag{16}$$

where the first and third terms represent the constant Doppler phase and Doppler modulation rate, respectively. Since they are independent of the range frequency f_τ, they do not cause range migration. The second and fourth terms represent linear range migration and second-order range curvature, respectively. These two terms correspond to the coupling components in (13) and (14), and thus become the key terms requiring compensation. As observed from (16), range migration is mathematically manifested as the linear coupling between f_τ and t_m, as well as the quadratic coupling between f_τ and t_m^2.

2) Generalized Second-order Keystone Transformation

To eliminate the second-order coupling term in (16), the generalized second-order Keystone transformation directly defines a new slow-time scaling variable as:

$$\begin{aligned}\tau_m &= \sqrt{\frac{f_c}{f_c + f_\tau}}\,t_m \\ t_m &= \sqrt{\frac{f_c + f_\tau}{f_c}}\,\tau_m\end{aligned} \tag{17}$$

Substituting (17) into the second-order range curvature term yields:

$$\begin{aligned}&-\frac{2\pi f_\tau}{c}a_k\left(\sqrt{\frac{f_c + f_\tau}{f_c}}\,\tau_m\right)^2 \\ &= -\frac{2\pi a_k}{c}f_\tau \cdot \frac{f_c + f_\tau}{f_c}\tau_m^2 \\ &= -\frac{2\pi a_k}{c}\frac{f_\tau(f_c + f_\tau)}{f_c}\tau_m^2\end{aligned} \tag{18}$$

Since $f_\tau \ll f_c$, it can be approximated that $\frac{f_\tau(f_c + f_\tau)}{f_c} \approx f_\tau$. Therefore, (18) can be simplified as $-\frac{2\pi a_k}{c}f_\tau\tau_m^2$ and the coupling between f_τ and τ_m^2 still exists. However, after this transformation, the phase term becomes linear with respect to the range frequency dimension. During discrete implementation, when performing IFFT along the range-frequency dimension to transform back to the range domain, the term $\exp\left(j\frac{2\pi a_k}{c}f_\tau\tau_m^2\right)$ is equivalent to a translation of the range envelope by $\Delta R = \frac{a_k}{2}\tau_m^2$. Since τ_m^2 is a deterministic slow-time function, this translation only depends on the acceleration a_k and is identical for all scattering centers of the same target. Therefore, it appears as an overall curvature of the target range trajectory rather than relative migration among scattering centers.In subsequent envelope alignment processing, this global

curvature can be removed through a global translation compensation.

Meanwhile, substituting (17) into the linear range migration term yields:

$$-\frac{4\pi f_\tau}{c} v_k \sqrt{\frac{f_c+f_\tau}{f_c}} \tau_m \approx -\frac{4\pi v_k}{c} f_\tau \tau_m \quad (19)$$

It can be observed that the linear range migration term is still compensated after the second-order Keystone transformation.After applying the generalized second-order Keystone transformation, the second-order range curvature has been corrected, and the remaining translational phase term in the echo mainly corresponds to the third term in (16):

$$-\frac{2\pi f_c}{c} a_k \tau_m^2 = -\frac{2\pi}{\lambda} a_k \tau_m^2 = \pi K_{a_k} \tau_m^2 \quad (20)$$

where $K_{a_k} = -\frac{2a_k}{\lambda}$ denotes the chirp rate.It can be seen that, after the transformation, the target echo in the slow-time domain is equivalent to an LFM signal. Its energy cannot be concentrated in the Fourier domain; however, a sharp peak can be obtained in the FrFT domain when the rotation angle matches the chirp rate.

3) Accurate Acceleration Estimation Based on FrFT

The p -order FrFT of the signal $x(t)$ is defined as:

$$X_p(u) = \int_{-\infty}^{\infty} x(t) K_p(u,t)\, dt \quad (21)$$

where the transform kernel $K_p(u,t)$ is given by

$$K_p(u,t) = A_\alpha \cdot \exp\left[j\pi \left(t^2 \cot\alpha - 2ut \csc\alpha + u^2 \cot\alpha \right) \right], \quad p \neq 2n \quad (22)$$

where $\alpha = \frac{p\pi}{2}$, and $A_\alpha = \sqrt{1 - j\cot\alpha}$. For an LFM signal $x(t) = \exp\left(j\pi K t^2 \right)$, when the fractional order p satisfies $\cot\alpha = -K \cdot \frac{N}{f_s}$, where N denotes the number of sampling points and f_s represents the sampling frequency, the quadratic phase term can be completely compensated. Consequently, the signal achieves maximum energy concentration in the FrFT domain. Combining with (23), the acceleration estimation equation can be obtained as:

$$a = -\frac{\lambda}{2} K_a = \frac{\lambda}{2} \cdot \frac{f_s}{N} \cot\alpha = \frac{\lambda}{2} \cdot \frac{f_s}{N} \cot\left(\frac{p\pi}{2} \right) \quad (23)$$

Since the acceleration a has a nonlinear relationship with the fractional order p according to (23), and the computational complexity of the discrete FrFT increases linearly with the number of searched fractional orders, performing a high-density search over the entire fractional order range would introduce considerable computational burden. Therefore, a coarse-to-fine two-stage search strategy is adopted.

The initial fractional order search range is defined as $p \in [p_{\min}, p_{\max}]$, where the range should cover the fractional orders corresponding to the possible maximum acceleration-induced chirp rates. A coarse step size Δp is employed for scanning. For each fractional order p_i, the transform-domain energy spectrum $\left| X_{p_i}(u) \right|^2$ is calculated. A focusing evaluation function is defined as the ratio between the power of the first M dominant peaks and the total signal power:

$$J(p_i)=\frac{\sum_{m=1}^{M}\left|X_{p_i}(u_m)\right|^2}{\sum_{u}\left|X_{p_i}(u)\right|^2} \tag{24}$$

This metric reflects the energy concentration degree of the LFM signal in the fractional Fourier domain. When the fractional order approaches the optimal value, $J(p_i)$ reaches its maximum. The L fractional orders corresponding to the largest evaluation values are recorded as candidate orders. After removing redundant candidates with excessively close intervals, the coarse acceleration estimation set is obtained as $\left\{\hat{p}_l^{(0)}\right\}_{l=1}^{L}$.

For each coarse estimation candidate $\hat{p}_l^{(0)}$, a second-stage search is performed within its neighborhood $\left[\hat{p}_l^{(0)}-\delta,\hat{p}_l^{(0)}+\delta\right]$ using a smaller step size Δp_m, yielding a refined focusing evaluation sequence $J(p)$. To overcome the limitation caused by discrete search intervals, a three-point parabolic interpolation method is employed to refine the peak location. Assuming that the peak index is i, and the adjacent evaluation values are J_{i-1},J_i and J_{i+1}, the sub-bin correction offset is given by:

$$\Delta i=\frac{1}{2}\cdot\frac{J_{i-1}-J_{i+1}}{J_{i-1}-2J_i+J_{i+1}} \tag{25}$$

Therefore, the refined optimal fractional order can be estimated as:

$$\hat{p}_l=p_i+\Delta i\cdot\Delta p_m \tag{26}$$

Substituting $\hat{p}_l$ into (23), the acceleration estimate corresponding to the l-th candidate can be obtained as $\hat{a}_l$. According to the coarse range trajectory model in (14), the quadratic coefficient satisfies $p_{k,2}=\frac{1}{2}\tilde{a}_k$, therefore, the coarse acceleration estimate can be expressed as $\tilde{a}_k=2p_{k,2}$. The FrFT search produces L candidate acceleration estimates $\{\hat{a}_l\}_{l=1}^{L}(L>K)$. To associate the FrFT candidates with actual targets, an association cost is defined as: $C_{l,k}=\left|\tilde{a}_l-\tilde{a}_k\right|$, and the optimal assignment is obtained by solving $\min_{\pi}\sum_{k=1}^{K}C_{\pi(k),k}$. Through this minimum-cost assignment strategy, the correspondence between each FrFT candidate and target identity is determined, and the accurate acceleration estimates of all targets are finally obtained as $\hat{a}_k$.

4) Velocity Recovery Based on First-order Keystone Transformation

After the FrFT-based processing in the previous section, the acceleration parameters of the targets can be accurately estimated. By utilizing the estimated acceleration parameters for secondary phase compensation, the second-order coupling between range frequency and slow time caused by acceleration can be effectively eliminated, allowing the target echo to approximately satisfy the uniform motion model again. At this stage, the dominant range migration in the target echo is mainly caused by velocity, which can be further compensated by employing the first-order Keystone transformation to achieve velocity recovery.

The range-compressed target echo can be expressed in the range-frequency and slow-time domain as:

$$\begin{aligned}&s_a(f_\tau,\tau_m)=s(f_\tau,\tau_m)\\&\exp\left[j\frac{2\pi}{c}(f_c+f_\tau)\hat{a}_k\tau_m^2\right]\end{aligned} \tag{27}$$

Since the actual target velocity may exceed the unambiguous velocity measurement interval, the echo may still contain range

migration caused by integer-folded velocity ambiguity. The velocity ambiguity interval is defined as $\Delta v = \frac{\lambda \cdot PRF}{2}$, where $PRF = \frac{1}{PRT}$ is the pulse repetition frequency. Therefore, the actual target velocity can be expressed as:

$$\hat{v} = \hat{v}_f + M\Delta\hat{v} \tag{28}$$

where v_f denotes the folded velocity, M represents the velocity ambiguity order. According to the difference between the estimated velocity obtained from the range trajectory and the folded velocity, the velocity ambiguity order can be determined by dividing the difference by the ambiguity interval and rounding to the nearest integer. A new virtual slow-time variable τ_m is introduced, and the scaling relationship is defined as:

$$\begin{aligned} \tau_m &= \frac{f_c}{f_c + f_\tau} t_m \\ t_m &= \frac{f_c + f_\tau}{f_c} \tau_m \end{aligned} \tag{29}$$

The first-order Keystone transformation is independent of the second-order Keystone transformation, and the two transformations can be applied to the echo signal in either order. Substituting (28) into the linear range migration term in (14) gives:

$$\begin{aligned} &-\frac{4\pi f_\tau}{c} v_k \cdot \frac{f_c + f_\tau}{f_c} \tau_m \\ &= -\frac{4\pi v_k}{c} \left(f_\tau \tau_m + \frac{f_\tau^2}{f_c} \tau_m \right) \end{aligned} \tag{30}$$

In wideband radar systems, the condition $f_\tau \ll f_c$ is generally satisfied. Therefore, the high-order term $\frac{f_\tau^2}{f_c}\tau_m \approx 0$ can be neglected, and (30) can be approximated as $-\frac{4\pi}{c} v_k f_\tau \tau_m$. At this point, although f_τ and τ_m are still multiplied together, τ_m is an independent virtual slow-time variable introduced by f_τ. Therefore, during the Fourier transform along the slow-time dimension, this phase term only results in a fixed Doppler shift and no longer causes range-cell migration due to variation of range frequency. After first-order Keystone correction, the first-order coupling between range frequency and slow time caused by velocity is effectively removed, and the target energy is re-concentrated into a fixed range cell. By performing Fourier transform along the corrected slow-time dimension, the target range–Doppler two-dimensional spectrum can be obtained. The Doppler peak location is searched within the corresponding range bin as:

$$\left(r, \hat{f}_d\right) = \arg\max \left| FFT\left[S_{KT}\left(r, \tau_m\right) \right] \right| \tag{31}$$

where $S_{KT}\left(r, \tau_m\right)$ denotes the echo data after first-order Keystone correction. According to the folded Doppler frequency corresponding to the detected peak position, the folded velocity can be obtained as $\hat{v}_f = -\frac{\lambda}{2}\hat{f}_d$. Finally, the true target velocity $\hat{v}_k$ is recovered by combining the integer velocity ambiguity order. After removing the estimated velocity and acceleration contributions from the coarse range trajectory, the mean value of the residual terms is calculated as:

$$\hat{R}_0 = \frac{1}{N} \sum_{n=1}^{N} \left[R\left(t_{m,n}\right) - \hat{v}_k t_{m,n} - \frac{1}{2} \hat{a}_k t_{m,n}^2 \right] \tag{32}$$

where N denotes the number of transmitted pulses. Finally, the complete target motion model is established as:

$$\hat{R}_k\left(t_m\right)=\hat{R}_0+\hat{v}_k t_m+\frac{1}{2}\hat{a}_k t_m^2 \quad (33)$$

B. Target-by-target Translational Motion Compensation and Signal Separation

1) Construction of Motion Compensation Function

Based on the motion parameter estimation in Section 3.1, the initial range, velocity, and acceleration of each target can be obtained, and the range motion trajectory of the k-th target described by (33) can be established. The range cell position corresponding to the m-th pulse of the k-th target can be expressed as:

$$n_k\left(t_m\right)=1+\frac{\hat{R}_k\left(t_m\right)-\hat{R}_k\left(0\right)}{\rho_a} \quad (34)$$

To avoid moving the target outside the data boundary, the median value of the range cells corresponding to the entire trajectory is selected as the reference range cell n_r. Therefore, the range translation amount required for the m-th pulse is:

$$\Delta n_k\left(t_m\right)=n_k\left(t_m\right)-n_r \quad (35)$$

A one-dimensional interpolation method is employed to achieve range envelope translation, ensuring that the target range envelope remains stable throughout the coherent processing interval. To suppress range sidelobe interference and interference from neighboring targets, a range gate is further applied around each target. Only the data within a certain range interval around the target is retained, thereby improving the stability of subsequent processing. In the implementation, the range cell position is calculated based on the estimated trajectory, and range interpolation compensation is performed pulse by pulse. Meanwhile, residual range data outside the target region are removed using a quadratic transition window to preserve the target echo.

After range envelope compensation, the target still contains common translational phase terms caused by radial velocity and radial acceleration. Therefore, according to the estimated motion parameters obtained in Section 3.1, the translational phase compensation function is constructed as:

$$H_k\left(t_m\right)=\exp\left[j\frac{4\pi}{\lambda}\left(\hat{v}_k t_m+\frac{1}{2}\hat{a}_k t_m^2\right)\right] \quad (36)$$

where the common phase term is $\phi_r\left(t_m\right)=-\frac{4\pi}{\lambda}\left(\hat{v}_k t_m+\frac{1}{2}\hat{a}_k t_m^2\right)$. This compensation removes the dominant common translational phase variations caused by the target's overall radial velocity and acceleration, allowing the Doppler migration of the target centroid to approach zero. Meanwhile, the differential Doppler information generated by the target's own rotational motion is preserved, which is essential for subsequent ISAR imaging.

2) Fine Envelope Alignment and Residual Phase Compensation

A reference range profile is first constructed by averaging the amplitudes of all received pulses:

$$p_r\left(r\right)=\frac{1}{M}\sum_{m=1}^{M}\left|s\left(r,m\right)\right| \quad (37)$$

Then, for each pulse, the translation amount is searched within a small range. For the m-th pulse, the range-cell translation is performed within the predefined search interval, and the correlation coefficient with the reference envelope is calculated as:

$$C\left(\Delta r\right)=\sum_r p_r\left(r\right)p_m\left(r+\Delta r\right) \quad (38)$$

where $p_m\left(r\right)$ represents the range envelope of the m-th pulse. The translation amount corresponding to the maximum correlation

coefficient is selected as the optimal compensation value: $\Delta r_m = \arg\max_{\Delta r} C(\Delta r)$. The obtained optimal translation amount is further compensated through interpolation, which can effectively remove the residual range-cell offset and improve the range focusing quality of the target.

Due to errors in motion parameter estimation and interpolation, residual range migration and common phase errors may still exist after compensation. Therefore, range-image correlation is further employed for fine alignment, and the residual nonlinear phase is estimated according to the strong scattering cells:

$$s_k'(r,t_m) = s_k(r,t_m)\exp\left[-j\phi_r(t_m)\right] \quad (39)$$

After phase compensation, the common phase of the current target is effectively removed, while the differential cross-range phase information generated by the target rotation is preserved. The compensated target echo energy is concentrated around a fixed range cell and Doppler region. Since different targets possess different motion parameters, their energy distributions remain separated in the range–Doppler plane. A range gate function $G_r(\cdot)$ and a Doppler gate function $G_d(\cdot)$ are constructed to perform joint gating on the compensated two-dimensional spectrum, retaining only the energy around the corresponding target:

$$s_s(r,t_m) = G_r(r)G_d(f_d)s_k'(r,t_m) \quad (40)$$

By compensating only one target at a time, the mutual interference caused by simultaneously compensating multiple targets can be avoided. Therefore, repeating the above procedure enables effective separation of multiple target signals.

C. ISAR Imaging and Global Coordinate Mapping

After target-by-target translational motion compensation and signal separation, the echo signal of each target satisfies the conventional RD imaging conditions. First, range compression is performed along the range direction. Then, a Blackman window is applied in the cross-range direction to suppress sidelobe interference, followed by Fourier transform along the slow-time dimension to obtain the ISAR image, i.e.

$$I(r,f_d) = \left|FFT\left[s_s(r,t_m)\right]\right| \quad (41)$$

Since the RD imaging result is represented in Doppler coordinates, a cross-range coordinate axis needs to be established according to the target motion parameters. Assuming that the instantaneous angular velocity of the target is $\omega = \frac{v_\perp}{R}$, the cross-range coordinate can be expressed as $x_c = -\frac{\lambda f_d}{2\omega}$. Therefore, the ISAR image coordinates can be transformed from (r,f_d) to (r,x_c) . An independent ISAR image is reconstructed for each target, and each image is initially represented in its own local coordinate system. According to the initial position and motion parameters of each target, the motion trajectory of the target in the global coordinate system can be recovered. The center position of the k -th target in the global coordinate system is defined as:

$$\mathbf{P}_k(t_m) = \begin{bmatrix} x_k(t_m) \\ y_k(t_m) \end{bmatrix} \quad (42)$$

where $x_k(t_m) = x_{0,k} + v_k t_m + \frac{1}{2}a_k t_m^2$, and $y_k(t_m)$ is defined similarly.

Based on the target center position, the unit vector along the target radial direction can be

further determined as

$$\mathbf{e}_r = \frac{\mathbf{P}_k - \mathbf{P}_r}{\left\| \mathbf{P}_k - \mathbf{P}_r \right\|} \tag{43}$$

where $\mathbf{P}_r$ denotes the radar position. The direction perpendicular to the range direction is defined as the cross-range direction, and its unit vector is expressed as:

$$\mathbf{e}_c = \begin{bmatrix} -e_{r,y} \\ e_{r,x} \end{bmatrix} \tag{44}$$

Therefore, any pixel (r, x_c) in the local ISAR image can be mapped to the global coordinate system as $\mathbf{P} = \mathbf{P}_k + x_c \mathbf{e}_c + r\mathbf{e}_r$. After coordinate transformation, each target image is interpolated onto a unified global grid, and image fusion is performed through amplitude accumulation to obtain the global multi-target ISAR image. Specifically, the procedure first determines the local coordinate axes of each target according to the estimated target motion parameters. Then, two-dimensional interpolation is employed to map the local ISAR image pixels onto the unified global coordinate grid. Finally, all target images are registered and fused to generate the global ISAR image of multiple targets.

IV. Simulation Experiments and Results Analysis

A. Simulation Setup

To validate the effectiveness of the proposed motion parameter estimation algorithm, simulations are conducted based on the multi-target echo model established in Section III. In the simulation scenario, three targets with different motion parameters are considered. Two targets maintain uniform motion, while the other target is subjected to radial acceleration, aiming to verify the adaptability of the proposed two-stage Keystone transformation and FrFT-based joint estimation method for high-speed maneuvering targets. A multi-target ISAR imaging simulation scenario containing three high-speed maneuvering targets is established to evaluate the performance of the proposed algorithm. An X-band radar system is adopted as the simulation platform, and the detailed parameter settings are listed in Table I.

TABLE I

System Simulation Parameters

Parameter	Value	Description
Carrier frequency	10GHz	X-band
Bandwidth	400MHz	Range resolution: 0.375
Pulse width	20μs	
PRF	200Hz	
Number of integrated pulses	1024	
Target 1 velocity	200m/s	0m/s^2
Target 2 velocity	250m/s	0m/s^2
Target 3 velocity	190m/s	-8m/s^2
Initial slant range	10km	

The simulation scenario contains three independent maneuvering targets, and each target is composed of five scattering centers. The spatial distributions of the scattering centers are illustrated in Fig. 3. Target 1 exhibits a cross-shaped configuration, Target 2 is arranged in an inverted T-shaped configuration, and Target 3 presents a tilted T-shaped configuration. The scattering amplitudes are randomly selected within the range of 4–8.

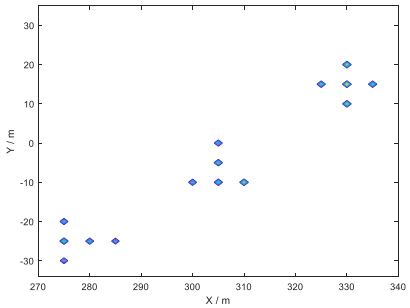
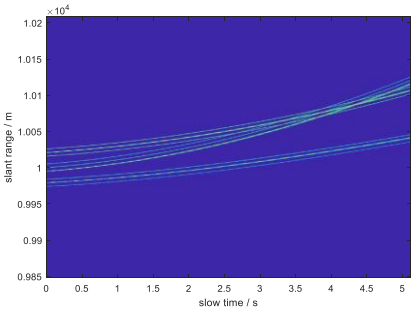


Fig. 3. Target scattering center model.

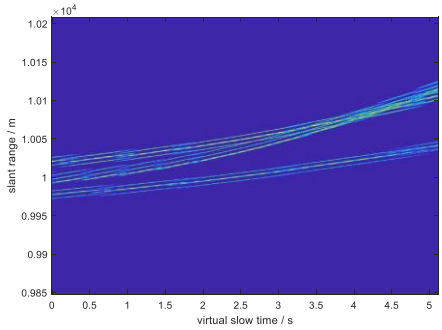
The three targets are spatially separated and possess different motion velocities and trajectories, providing a representative simulation scenario for multi-target ISAR imaging.

B. Analysis of Imaging Results

The generalized second-order Keystone transformation is first applied to the range-compressed data to correct the second-order range curvature induced by target acceleration. The range–slow-time images before and after compensation are compared, as shown in Fig. 4(b) and Fig. 4(c).



(a)Before generalized second-order Keystone transformation



(b)After generalized second-order Keystone transformation

Fig. 4. Range–slow-time profiles of mixed target echoes before and after generalized second-order Keystone transformation.

It can be observed that, before compensation, all targets exhibit apparent range migration. Specifically, the third target suffers from radial acceleration, resulting in an obvious second-order curved range trajectory, whereas the other two targets exhibit approximately linear range migration trajectories. After applying the generalized second-order Keystone transformation, the range curvature of the targets is effectively corrected, and the range trajectories become approximately straight lines. This provides favorable conditions for the subsequent accurate acceleration estimation using the FrFT. Since the second-order coupling between range frequency and slow time is effectively eliminated, the target echo energy becomes more concentrated, demonstrating that the proposed transformation can effectively suppress the range curvature effect caused by acceleration.

After the second-order range curvature compensation, the compensated target echoes are processed by the FrFT. The optimal fractional order is searched according to the energy concentration degree of the target in different fractional-order domains, and the target radial acceleration is recovered according to the optimal fractional order. To balance computational efficiency and estimation accuracy, a two-stage search strategy combining coarse search and fine search is adopted. First, a relatively large search step is used to determine the candidate fractional orders. Then, a fine search is performed around each candidate order, and parabolic interpolation is employed to further improve the acceleration estimation accuracy.

For multiple targets, the candidate peaks obtained from the FrFT search cannot be directly associated with target identities.

Therefore, the coarse acceleration estimates obtained from the range trajectory fitting are combined to establish a minimum-cost association criterion, achieving a one-to-one correspondence between FrFT candidates and target trajectories. This strategy not only improves the acceleration estimation accuracy but also avoids incorrect matching of candidate peaks in multi-target scenarios.

After obtaining the target acceleration estimates, the second-order phase terms in the echoes are compensated, allowing the target echoes to approximately satisfy the uniform motion model. Subsequently, the first-order Keystone transformation is employed to correct the range migration caused by radial velocity. The Doppler spectrum is then obtained through Fourier transform along the slow-time dimension, and the target radial velocity is recovered according to the Doppler peak.

For targets with velocity ambiguity, the ambiguity order is determined by combining the coarse trajectory estimation results, thereby recovering the true radial velocity. By jointly estimating velocity and acceleration, a complete target motion model can be established, providing accurate motion parameters for subsequent target-dependent translational motion compensation and echo separation.

Table II

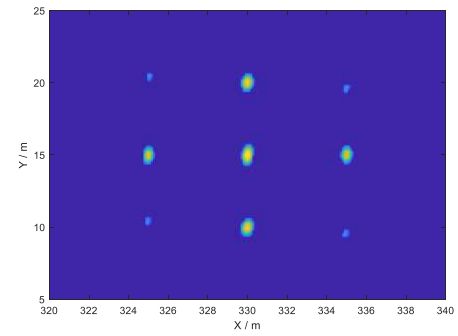
Motion parameter estimation results.

Target	1	2	3
True velocity(m/s)	200	250	190
Estimated velocity (m/s)	200.128	250.516	190.281
True acceleration(m/s^2)	0	0	-8
Estimated acceleration(m/s^2)	-0.062	-0.089	-7.592

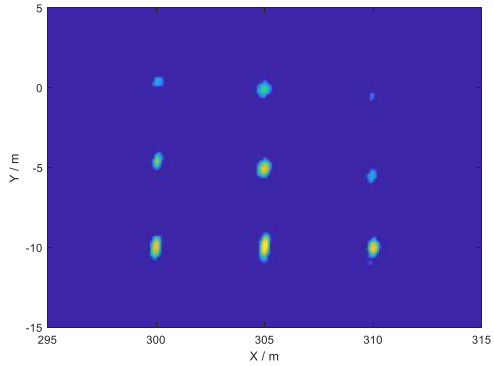
Table II presents the comparison between the estimated target motion parameters obtained by the proposed algorithm and the corresponding true values. It can be observed that the radial velocity and radial acceleration of all three targets are accurately estimated. For the two uniformly moving targets, the velocity estimation errors are relatively small. For the maneuvering target, the estimated acceleration is highly consistent with the true value, demonstrating that the generalized second-order Keystone transformation can effectively correct the range curvature induced by acceleration, while the FrFT can accurately recover the target chirp rate and achieve precise estimation of the radial acceleration of high-speed maneuvering targets. Meanwhile, the first-order Keystone transformation further eliminates the range migration caused by target velocity and enables accurate velocity recovery, providing reliable motion parameters for subsequent target separation and ISAR image formation.

To further validate the effectiveness of the proposed target-dependent translational compensation and signal separation method, the estimated motion parameters obtained in Section 3.2 are utilized to perform range envelope correction, translational phase compensation, and residual error compensation for each target.

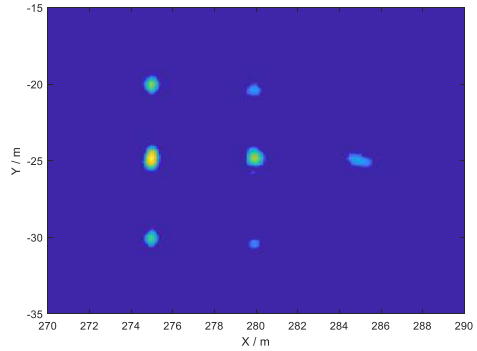
A two-dimensional gating function is applied in the range–Doppler domain to extract the echo corresponding to each target. In the cross-range direction, a Blackman window is first applied to suppress sidelobes. Subsequently, Fourier transform is performed along the slow-time dimension to obtain the range–Doppler images of the three targets, as shown in Fig. 5.



(a) ISAR image of Target 1



(b) ISAR image of Target 2



(c) ISAR image of Target 3

Fig. 5. ISAR images of multiple targets.

A further comparison of the imaging results of the three targets demonstrates that, due to the differences in motion parameters and spatial positions, the local ISAR images of the three targets preserve their respective scattering characteristics. For the uniformly moving targets, the scattering centers remain stable and the images achieve good focusing quality. For the maneuvering target with radial acceleration, the range curvature is effectively suppressed after applying the generalized second-order Keystone transformation and FrFT-based acceleration compensation, enabling the target to obtain satisfactory focusing performance. These results verify that the proposed motion compensation method has good adaptability for maneuvering target ISAR imaging. The local ISAR images of the three targets obtained in Section 4.4 are further mapped into a unified global coordinate system, and multi-target image fusion is performed. The final global coordinate reconstruction result is shown in Fig. 6.

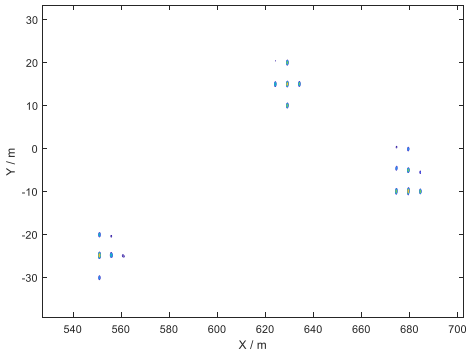


Fig. 6. Global coordinate reconstruction of multi-target ISAR images.

V. Conclusion

This paper investigates the challenges in multi-target ISAR imaging under high-speed maneuvering conditions, including severe range migration, difficulty in motion parameter separation, and mutual interference among multiple target echoes. A multi-target ISAR imaging and global localization method based on an improved Keystone transformation and FrFT-based joint processing is proposed.

First, range peak detection is performed after range compression to obtain the range trajectories of multiple targets. A second-order polynomial fitting model is then established to provide prior constraints for subsequent parameter estimation. To address the second-order range curvature caused by high-speed maneuvering targets, a generalized second-order Keystone transformation is introduced to effectively eliminate the second-order coupling

between range frequency and slow time. Subsequently, by exploiting the slow-time modulation characteristics induced by acceleration, the FrFT-domain energy concentration property is utilized to estimate the radial acceleration. Combined with coarse trajectory estimation, a multi-target candidate peak association strategy is developed to achieve accurate acceleration estimation. Furthermore, acceleration compensation and first-order Keystone transformation are employed to recover the true radial velocity of each target, enabling joint estimation of velocity and acceleration parameters.

Secondly, based on the estimated target motion parameters, the range envelope compensation and common translational phase compensation functions are constructed for each target. The target echoes are refocused in the range–Doppler domain, and multiple target signals are separated by employing range and Doppler gating. Finally, the local ISAR images of all targets are mapped into a unified global coordinate system, enabling multi-target ISAR image fusion and spatial position reconstruction.

Simulation results demonstrate that the proposed method can effectively estimate the motion parameters of high-speed maneuvering targets. The velocity estimation errors of the three targets are relatively small, and the estimated acceleration of the maneuvering target remains highly consistent with the true value. Meanwhile, clear target ISAR images are obtained and global coordinate reconstruction is achieved. These results verify the effectiveness of the proposed method for multi-target high-speed maneuvering ISAR imaging scenarios.

References

[1] BAO Z, XING M D, and WANG T. Radar Imaging Technology[M]. Beijing, China: Publishing House of Electronics Industry, 2005.

[2] CHEN V C, LING H. Time-Frequency Transforms for Radar Imaging and Signal Analysis [M]. Boston: Artech House, 2002.

[3] WEHNER D R. High-Resolution Radar[M]. 2nd ed. Boston: Artech House, 1995.

[4] WANG J N, HUANG P H, MA J T, et al. A novel ISAR imaging approach for moving targets utilizing joint particle swarm optimization and time polynomial rescaling-nonuniform FFT[J]. IEEE Geoscience and Remote Sensing Letters, 2024, 21: 1-5.

[5] DING J B, WANG J D, LI Y C, et al. An efficient ISAR imaging and scaling method for highly maneuvering targets based on ICPF-PSVA[J]. IEEE Transactions on Geoscience and Remote Sensing, 2024, 62: 1-15.

[6] YANG T, SHI H Y, GUO J W, et al. ISAR imaging for maneuvering target based on suitable CPI extraction and PC-MBSBL[J]. IEEE Transactions on Aerospace and Electronic Systems, 2024, 60(6):8118-8135.

[7] JIANG Y C, NI H, CHEN R D, et al. Translational motion compensation method for ISAR imaging of air maneuvering weak targets based on CV-GRUNet[J]. IEEE Geoscience and Remote Sensing Letters, 2024, 21:1-5.

[8] YANG S H, LI S Q, FAN H T, et al. High-resolution ISAR imaging of maneuvering targets based on azimuth adaptive partitioning and compensation function estimation[J]. IEEE

Transactions on Geoscience and Remote Sens ing, 2023, 61:1-15.

[9] DING J B, LI Y C, WANG J D, et al. Inte gration of high-order motion compensation an d 2-D scaling for maneuvering target bistatic ISAR imaging[J]. IEEE Transactions on Geos cience and Remote Sensing, 2025, 63:1-20.

[10] YANG J X, WANG Y, et al. Sparse aperture inverse synthetic aperture radar imaging for maneuvering targets with migration through r esolution cells correction[J]. IEEE Journal of Selected Topics in Applied Earth Observation s and Remote Sensing, 2025,18:4446-4472.

[11] SHI. H Y, LIU Y, Guo J, et al. ISAR autofo cus imaging algorithm for maneuvering target s based on deep learning and keystone transf orm[J]. Journal of Systems Engineering and Electronics,2020,30(6):1178-1185.

[12] XIN H C, BAI X, SONG Y E, et al. ISAR imaging of target with complex motion associ ated with the fractional Fourier transform[J]. Digital Signal Processing, 2018, 83:332-345.

[13] ZHAO J, ZHANG M, WANG X, et al. Para meters estimation and ISAR imaging of multi ple maneuvering targets based on an order re duction method for cubic chirps[J]. Journal of electromagnetic waves and applications, 201 7, 31(16):1658-1675.

[14] CHEN S Y, HU W H, GUO B F , et al.The Current Situation and Development of Multit arget ISAR Imaging[C]//2025 17th Internation al Conference on Signal Processing Systems (ICSPS), Chengdu, China, 2025: 1196-1201.

[15] CHEN S Y, ZHANG Y H, YANG J F, et al. ISAR imaging algorithm for maneuvering tar get sequences based on FrFT and Kalman filt ering[J]. Remote Sensing Technology and Ap plication, 2024,39(5): 1196–1204.

[16] ZHOU, A.; YANG, Q.; YUAN, Z A.; WAN G, H Q, et al. Spaceborne THz-ISAR Imagin g of Space Target with Joint Motion Compen sation Based on FrFT and GWO[J]. Remote Sens, 2025, 17, 2152.

[17] TANG B, WANG H Q, YANG Q, et al. Hig h-Order Rotational-Migration Correction and I SAR Imaging in the THz Band Considering I mpact of Scattering Intensity[J]. IEEE Transa ctions on Geoscience and Remote Sensing, 2 024, 62:1-11.

Declarations

Funding: Hebei Natural Science Foundation Gener al Program (Grant No. F2019506031)

Project Title: Research on Sparse Aperture Fusion Imaging Technology for Space Targets Based on T/R-R Radar

Author contribution:



Siyuan Chen(2001.07-) is currently pursuing the M.S. degree at the Shijiazhuang Campus, Army Engineering University, Shijiazhuang 050003, China. His research interests include inverse synthetic aperture radar imaging and radar motion compensation. **Wenhua Hu**(1970.08-) is an Associate Professor with the Shijiazhuang Campus, Army Engineering University, Shijiazhuang 050003, China. His research interests focus on radar signal processing, multi-target ISAR imaging and low-SNR motion compensation algorithms. His e-mail is cccg00630@163.com. **Baofeng Guo**(1987.07-) is a Lecturer with the Shijiazhuang Campus, Army

Engineering University, Shijiazhuang 050003, China. His research interests include radar echo simulation, range envelope alignment and ISAR image reconstruction.**Dongfang Xue**(1983.11-) is a Lecturer with the Shijiazhuang Campus, Army Engineering University, Shijiazhuang 050003, China. His research interests cover radar target detection and translational motion compensation.**Miao Li**(1991.02-) is a Lecturer with the Shijiazhuang Campus, Army Engineering University, Shijiazhuang 050003, China. His research interests include multi-target radar signal separation and low-SNR imaging technology.